Origin of strain-induced resonances in flexible terahertz metamaterials*

Xiu-Yun Sun(孙秀云)[1], Li-Ren Zheng(郑立人)[2], Xiao-Ning Li(李枭宁)[1], Hua Xu(徐华)[1,†], Xian-Ting Liang(梁先庭)[1], Xian-Peng Zhang(张贤鹏)[2], Yue-Hui Lu(鲁越晖)[2,‡], Young-Pak Lee[3], Joo-Yull Rhee[4], and Wei-Jie Song(宋伟杰)[2]

[1] *Department of Physics and Institute of Optics, Ningbo University, Ningbo* 315211, *China*
[2] *Ningbo Institute of Material Technology and Engineering, Chinese Academy of Sciences, Ningbo* 315201, *China*
[3] *Department of Physics and RINS, Hanyang University, Seoul* 133-791, *Korea*
[4] *Department of Physics, Sungkyunkwan University, Suwon* 440-746, *Korea*

(Received 18 December 2015; revised manuscript received 16 January 2016; published online 5 April 2016)

Two types of flexible terahertz metamaterials were fabricated on polyethylene naphthalate (PEN) substrates. The unit cell of one type consists of two identical split-ring resonators (SRRs) that are arranged face-to-face (i.e., FlexMetaF); the unit cell of the other type has nothing different but is arranged back-to-back (i.e., FlexMetaB). FlexMetaF and FlexMetaB illustrate the similar transmission dips under zero strain because the excitation of fundamental inductive–capacitive (LC) resonance is mainly dependent on the geometric structure of individual SRR. However, if a gradually variant strain is applied to bend FlexMetaF and FlexMetaB, the new resonant peaks appear: in the case of FlexMetaF, the peaks are located at the lower frequencies; in the case of FlexMetaB, the peaks appear at the frequencies adjacent to the LC resonance. The origin and evolution of strain-induced resonances are studied. The origin is ascribed to the detuning effect and the different responses to strain from FlexMetaF and FlexMetaB are associated with the coupling effect. These findings may improve the understanding on flexible terahertz metamaterials and benefit their applications in flexible or curved devices.

Keywords: flexible terahertz metamaterials, split ring resonator, strain, resonance

PACS: 78.67.Pt, 42.60.Da, 42.25.Bs **DOI:** 10.1088/1674-1056/25/5/057802

1. Introduction

Metamaterials, artificial sub-wavelength scale structures, are receiving increasing attention because of their exotic properties, such as negative refraction, super focusing, and invisible cloaking.[1–3] Recently, metamaterials scaled to operate at the terahertz (THz) frequency have attracted a great deal of interest. Moser *et al.* realized the first THz metamaterials according to Pendry's report.[4] Chen *et al.* presented an efficient active metamaterial switch/modulator electrically connecting the individual metamaterial elements operating at THz frequencies.[5] Moreover, THz metamaterials have great prospects in other applications, such as chemical and biological sensors, absorbers, modulator, and slow light devices.[6–9]

Split-ring resonators (SRRs) are most often used as building blocks for microwave, THz, and infrared metamaterials.[10–13] SRRs were first introduced by Pendry *et al.*[14] as an important optical component for metamaterials, which may exhibit both electric and magnetic resonances. Most studied planar metamaterials based on double SRRs have symmetric structures.[15] More interestingly, once the symmetry of the double SRR structure is broken, it is possible to find some new fascinating effects, such as an electromagnetically induced transparency (EIT) effect and Fano resonance.[6,16,17] In terms of THz metamaterials, few efforts are made on flexible counterparts and such studies usually focus on the mechanical effects on ordinary inductive–capacitive (LC) resonance.[18,19] Though we have observed the strain-induced resonances in flexible THz metamaterials,[20] the underlying origin of the interaction mechanism between the resonances and strain has not been well understood.

In this work, we fabricate two types of flexible THz metamaterials, FlexMetaF and FlexMetaB. The unit cells of FlexMetaF and FlexMetaB consist of two identical SRRs, with the face-to-face and back-to-back arrangements, respectively. FlexMetaF and FlexMetaB demonstrate the different THz electromagnetic responses if a strain was applied, though they show the similar LC resonance without strain. The effects of detuning and coupling are comprehensively investigated to elucidate the roles of strain, which may improve the understanding on the interaction between strain and the electromagnetic response in flexible terahertz metamaterials in terms of their applications in flexible or curved devices.

*Project supported by the National Natural Science Foundation of China (Grant Nos. 11204146 and 61574144), the Ningbo Key Laboratory of Silicon and Organic Thin Film Optoelectronic Technologies, China, the Program for Ningbo Municipal Science and Technology Innovative Research Team, China (Grant No. 2015B11002), and the K. C. Wong Magna Foundation in Ningbo University, China.

†Corresponding author. E-mail: xuhua@nbu.edu.cn
‡Corresponding author. E-mail: yhlu@nimte.ac.cn

© 2016 Chinese Physical Society and IOP Publishing Ltd

2. Simulation and experiment

2.1. Simulation

To model the THz response of metamaterials, the numerical simulations are carried out using a finite integration package (CST Microwave Studio). Two types of metamaterials are designed: one consists of two SRRs face-to-face; the other has nothing different but the two SRRs were arranged back-to-back, which are named as FlexMetaF and FlexMetaB, respectively (see Figs. 1(a) and 1(b)). The detailed geometric parameters are $L = 30$ μm, $S = 12$ μm, and $G_1 = G_2 = W = 6$ μm. The permittivity of the silver SRRs is represented using a Drude model with a plasma frequency of $\omega_p = 1.366 \times 10^{16}$ rad/s and a collision frequency of $\omega_c = 4 \times 10^{13}$ Hz[20] and the nickel is modeled as a lossy metal with a conductivity of 3.3×10^6 Sm^{-1}.[21] The permittivity of polyethylene naphthalate (PEN) substrates is taken to be 2.56.[22] Periodic and open boundary conditions are applied to the x and y directions, and the z direction, respectively. The periodicities in the x and y directions are 96 μm and 66 μm, respectively. The incident THz waves are linearly polarized along the y direction.

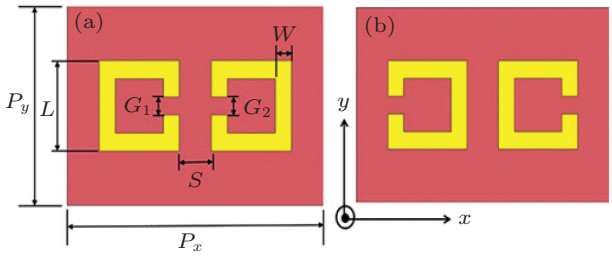


Fig. 1. (color online) Representation of the unit cell of (a) FlexMetaF and (b) FlexMetaB. The geometric parameters are $L = 30$ μm, $S = 12$ μm, $G_1 = G_2 = W = 6$ μm, $P_x = 96$ μm, and $P_y = 66$ μm. The electric field component of THz waves is along the y direction.

2.2. Fabrication

According to the designed structures, FlexMetaF and FlexMetaB were prepared on the 75-μm-thick PEN substrates by standard photolithography. Followed by electron beam evaporation (EBE), a 10-nm-thick nickel and 200-nm-thick silver layers were deposited, in which the nickel layer was used to enhance the adhesion of silver to PEN substrates. Finally, the patterned photoresist and the redundant metal were removed through a lift-off process.

2.3. Characterization

The surface morphologies of the flexible terahertz metamaterials were characterized using an optical microscope (Leica DM2500M, Germany). A THz time-domain spectroscopy (THz–TDS) system was employed to measure the transmission amplitudes, which were normalized to that of the reference PEN substrates as $|t(\omega)| = |t_s(\omega)/t_R(\omega)|$. Here, $t_s(\omega)$ and $t_R(\omega)$ are transmission of samples and substrates, respectively.[23] A custom-made bending equipment was used to bend the samples with a high precision and good repeat ability by adjusting the micrometer gauge.[20]

3. Results and discussion

Figures 2(a) and 2(b) show the surface morphologies of FlexMetaF and FlexMetaB, respectively, in which the designed structures were experimentally realized without obvious imperfections. The overall size of the samples is approximately 15×20 mm^2, which accommodates ten thousands of unit cells. The measured and simulated transmission spectra of FlexMetaF and FlexMetaB under zero strain are shown in Figs. 2(c) and 2(d), respectively. Both of them reveal the similar transmission dips, which originate from the excitation of fundamental LC resonance. The resonant frequency is mainly governed by the geometric structure of individual SRR and less dependent on specific configurations of SRRs (e.g., face-to-face or back-to-back arrangement) in our experiment. Compared with the simulation results, the measured LC resonance was slightly blue-shifted, which could be attributed to the preparation imperfection and the permittivity deviation from that used in simulations.

To investigate the effects of bending strain on THz electromagnetic response, the fabricated flexible metamaterials were mounted onto the custom-made bending equipment. The description of applied strain ε can be found in Ref. [20]. The THz–TDS measurements were performed when FlexMetaF and FlexMetaB were bent, as shown in Figs. 3(a) and 3(b), respectively, where the stress was applied to be perpendicular to the gaps of SRRs for breaking the symmetry of two SRRs in the unit cell. The changes in the distance between the two clamps of the bending equipment increase from 0 to 2.5 mm with an increment of 0.5 mm, corresponding to the applied strain ε of 0, 2.86‰, 4.05‰, 4.96‰, 5.73‰, and 6.41‰, respectively. The transmission spectra of the bent FlexMetaF and FlexMetaB are presented in Figs. 3(c) and 3(d), respectively, where FlexMetaF and FlexMetaB show the robust THz responses under strain. Though it is noted that the strain has no obvious effects on the transmission spectra, the small strain-induced resonances appear, as denoted by the rectangles in Figs. 3(c) and 3(d). For FlexMetaF, the strain-induced resonant peaks appear at around 1.2 THz, which are located at the lower frequencies than that of the LC resonance; for FlexMetaB, the strain-induced peaks are almost located at the frequency of the LC resonance, 1.3 THz. It is believed that the strain-induced resonances may be associated with the involved detuning and/or coupling effects,[24,25] which have different influences on FlexMetaF and FlexMetaB.

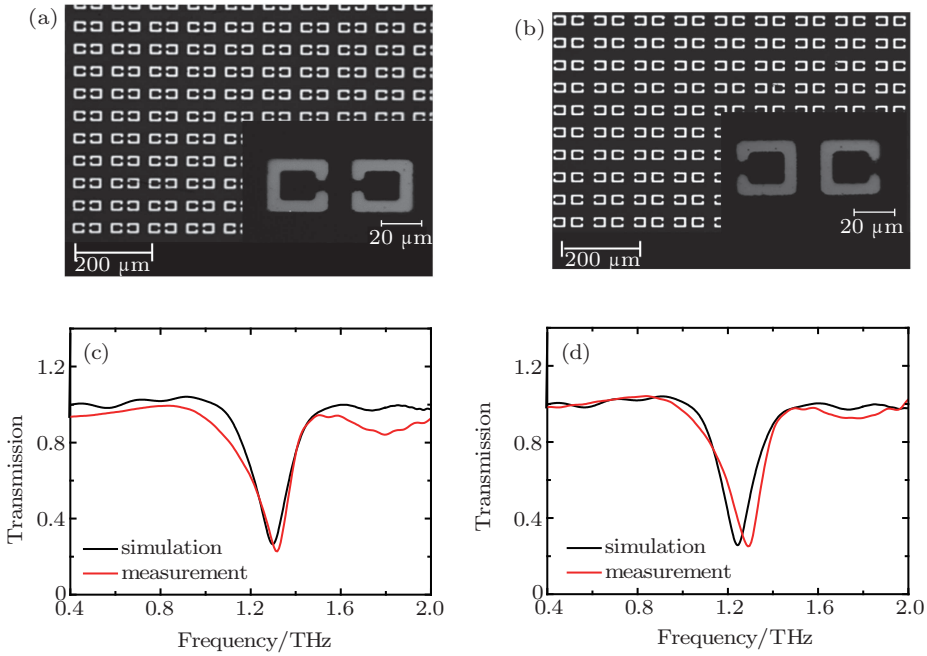


Fig. 2. (color online) Optical microscope images of (a) FlexMetaF and (b) FlexMetaB. Measured (red) and simulated (black) transmission spectra of (c) FlexMetaF and (d) FlexMetaB without any bending strain.

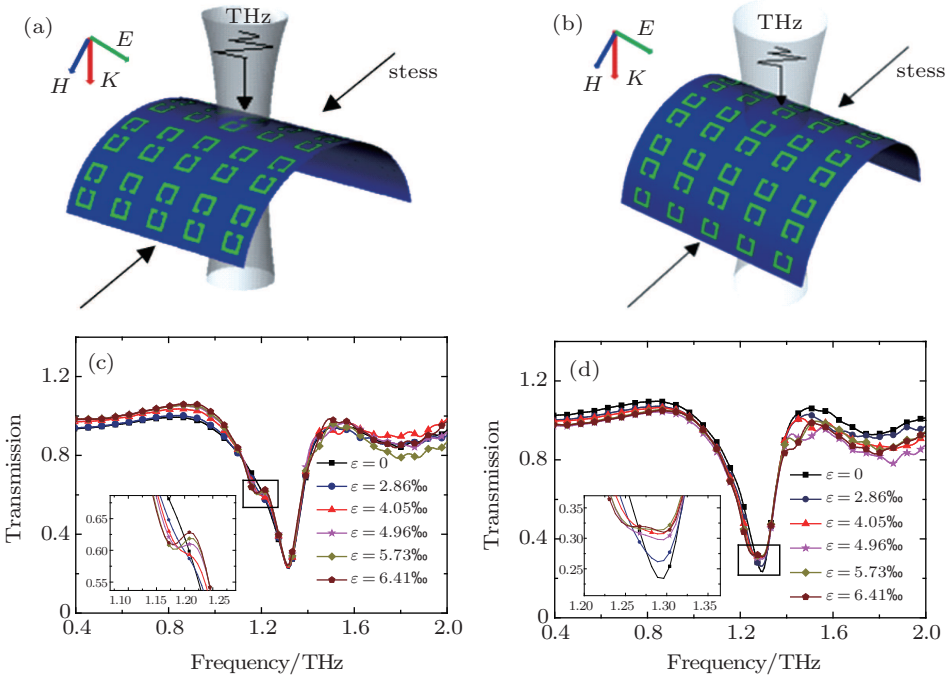


Fig. 3. (color online) Experimental schematic of (a) FlexMetaF and (b) FlexMetaB under bending strain. The corresponding measured transmission spectra of (c) FlexMetaF and (d) FlexMetaB under the bending strain varying from 0 to 6.41‰. Inset: zoom-in view of the strain-induced resonances under the various bending strains.

To find out the origin of strain-induced resonances, the detuning effects on FlexMetaF and FlexMetaB are investigated by artificially taking the different gap sizes of the two SRRs. Because it is almost unlikely to quantitatively simulate the bent metamaterials due to the unavailability of periodic conditions and tremendous computation resources, varying gap size is a route to introduce the detuning effects. Figures 4(a) and 4(b) show the transmission spectra of FlexMetaF and FlexMetaB, respectively, with the invariant left SRR and the varied right SRR ($G_2 = 6$, 3.6, 3.4, 3.2 μm). FlexMetaF shows the asymmetry-induced peaks at the lower frequencies, whereas FlexMetaB has the peaks adjacent to the LC resonant frequency, which is in agreement with the experimental observation. Although the strain-induced resonances in the flexible metamaterials cannot be simply equivalent to the varied gap size, it will not lose generality as a way to introduce the detun-

ing effects and study these effects on the THz electromagnetic response.

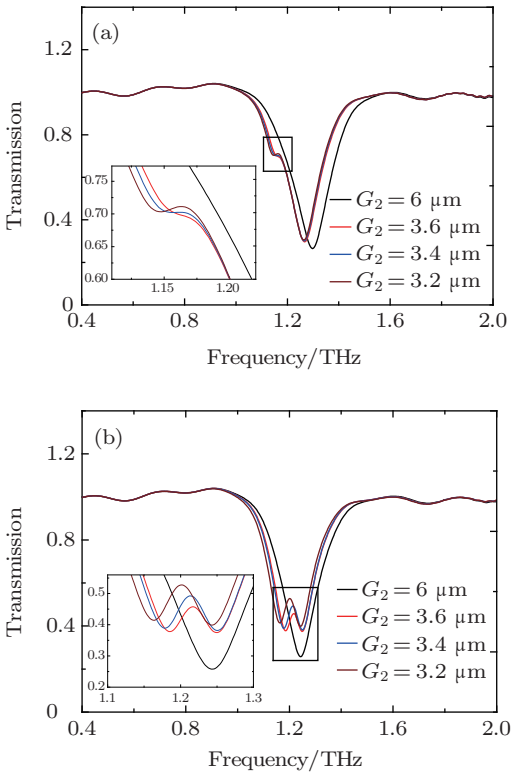


Fig. 4. (color online) Simulated transmission spectra of (a) FlexMetaF and (b) FlexMetaB, with the gap width of the right SRR $G_2 = 6$, 3.6, 3.4, 3.2 μm. Inset: zoom-in view of the resonant peaks.

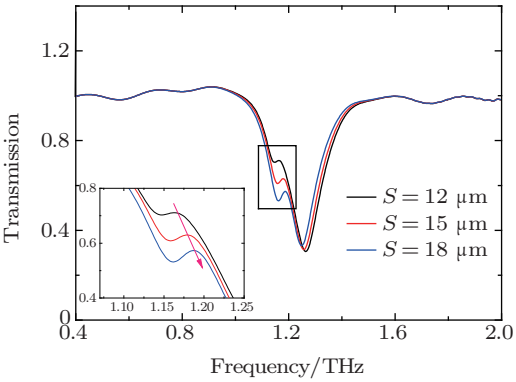


Fig. 5. (color online) Simulated transmission spectra of FlexMetaF with different coupling distances S when the right SRR has a gap width of $G_2 = 3.2$ μm. Inset: zoom-in view of the blue-shifted resonant peaks, as denoted by the arrow.

On the other hand, the frequency difference of the strain-induced resonances between FlexMetaF and FlexMetaB might be ascribed to the coupling strength, since it is dependent on the gap distance of two SRRs. Figure 5 shows the transmission spectra of the variant FlexMetaF with $G_1 = 6$ μm and $G_2 = 3.2$ μm with various distances of two SRRs, S, which increases from 12 to 18 μm with an increment of 3 μm. The detuning-induced resonances experience a blueshift with increasing S, which implies that such resonances have higher frequencies in weakly-coupled SRR metamaterials and lower frequencies in strongly-coupled ones. It explains that the bent FlexMetaF shows the strain-induced resonances at the lower frequencies due to the stronger coupling between two SRRs resulting from the face-to-face arrangement, as compared to the weakly coupled SRRs with the back-to-back arrangement in FlexMetaB.

To investigate the underlying origin of strain-induced resonances in a more general way, the harmonic oscillator model is used to study the effects of detuning and coupling, where the indirect coupling was considered.[9,26] The incident electric field is $\boldsymbol{E} = \boldsymbol{E}_0 \mathrm{e}^{\mathrm{i}\omega t}$, and two particles have the same effective charge and mass ($q_1 = q_2 = q$, $m_1 = m_2 = m$). The equations of motion are expressed as

$$\begin{aligned} \ddot{\boldsymbol{x}}_1 + \gamma\dot{\boldsymbol{x}}_1 + \omega_0^2\boldsymbol{x}_1 + \kappa\boldsymbol{x}_2 &= \frac{q}{m}\boldsymbol{E}, \\ \ddot{\boldsymbol{x}}_2 + \gamma\dot{\boldsymbol{x}}_2 + (\omega_0+\delta)^2\boldsymbol{x}_2 + \kappa\boldsymbol{x}_1 &= \frac{q}{m}\boldsymbol{E}, \end{aligned} \tag{1}$$

where ω_0 and $\omega_0 + \delta$ are the resonant frequencies of two oscillators, respectively, and δ is the detuning frequency. k and γ are the coupling coefficient between two oscillators and the damping rate, respectively. Solving the above coupled equation (1) for $\boldsymbol{x}_1$ and $\boldsymbol{x}_2$, the following equations are obtained:

$$\boldsymbol{x}_1 = \frac{q}{m}\boldsymbol{E}\frac{(\omega_0+\delta)^2 - \omega^2 + \mathrm{i}\gamma\omega - \kappa}{(\omega_0^2 - \omega^2 + \mathrm{i}\gamma\omega)[(\omega_0+\delta)^2 - \omega^2 + \mathrm{i}\gamma\omega] - \kappa^2}, \tag{2}$$

$$\boldsymbol{x}_2 = \frac{q}{m}\boldsymbol{E}\frac{\omega_0^2 - \omega^2 + \mathrm{i}\gamma\omega - \kappa}{(\omega_0^2 - \omega^2 + \mathrm{i}\gamma\omega)[(\omega_0+\delta)^2 - \omega^2 + \mathrm{i}\gamma\omega] - \kappa^2}. \tag{3}$$

The linear susceptibility (χ), which relates the polarization ($\boldsymbol{P}$) of the particle to the strength of incident electric field ($\boldsymbol{E}$), is expressed in terms of the displacement vectors as follows:

$$\chi = \frac{\boldsymbol{P}}{\varepsilon_0\boldsymbol{E}} = \frac{q(\boldsymbol{x}_1 + \boldsymbol{x}_2)}{\varepsilon_0\boldsymbol{E}}, \tag{4}$$

$$\chi = \frac{q^2}{\varepsilon_0 m} \times \frac{\omega_0^2 + (\omega_0+\delta)^2 - 2\omega^2 + \mathrm{i}2\gamma\omega - 2\kappa}{(\omega_0^2 - \omega^2 + \mathrm{i}\gamma\omega)[(\omega_0+\delta)^2 - \omega^2 + \mathrm{i}\gamma\omega] - \kappa^2}. \tag{5}$$

The real part of susceptibility ($\mathrm{Re}[\chi]$) represents the dispersion and the imaginary part ($\mathrm{Im}[\chi]$) gives the absorption (loss) within the medium. To compare with the transmission spectra, $1 - |\mathrm{Im}[\chi]|$ is presented in Fig. 6. Figure 6(a) shows the spectra for various detuning frequencies δ, taking the parameters as $\gamma = 4 \times 10^{-2}$,[27] $\kappa = 5 \times 10^{-2}$, $\omega_0 = 1.3$, and $q^2/(\varepsilon_0 \times m) = 2.5 \times 10^{-2}$. It is observed that the new resonant peaks appear if the detuning effects are introduced and the resonance peaks are located at the lower frequencies, as compared with non-detuned LC resonance. This verifies that the strain-induced resonances originate from the detuning effects. Varying the coupling strength κ, $1 - |\mathrm{Im}[\chi]|$ is plotted in Fig. 6(b), where $\gamma = 4 \times 10^{-2}$, $\delta = -0.05$, $\omega_0 = 1.3$, and $q^2/(\varepsilon_0 \times m) = 2.5 \times 10^{-2}$. With increasing coupling strength,

the new resonance is red-shifted, as observed from Fig. 6(b). Therefore, the differences of the strain-induced resonances between FlexMetaF and FlexMetaB could be ascribed to different coupling strengths due to the different gap distances between the two SRRs.

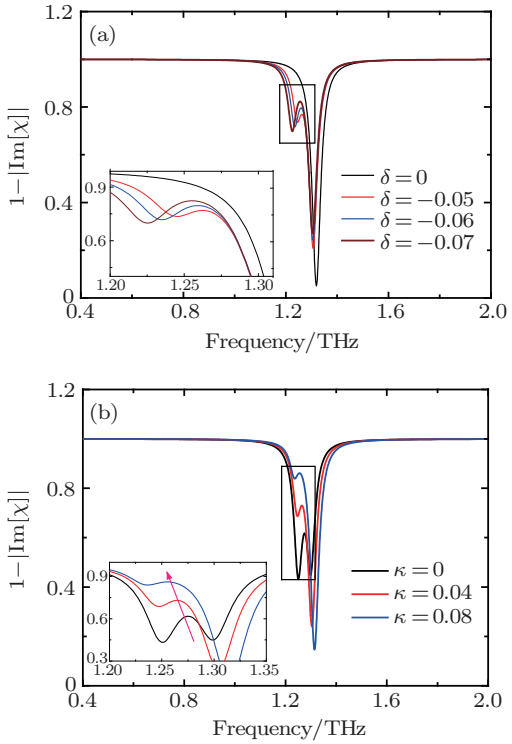


Fig. 6. (color online) Dependences of $1-|\mathrm{Im}[\chi]|$ on (a) the detuning frequency and (b) the coupling strength. Inset of panel (a): zoom-in view of the resonant peaks. Inset of panel (b): zoom-in view of the red-shifted resonant peaks with the coupling strength κ increasing, as denoted by the arrow.

4. Conclusions

In this work, two types of flexible THz metamaterials, FlexMetaF and FlexMetaB, were fabricated on the PEN substrates. The unit cells of FlexMetaF and FlexMetaB consist of two identical SRRs with a different arrangement, where the former and the latter were arranged face-to-face and back-to-back, respectively. The similar THz electromagnetic responses was observed from FlexMetaF and FlexMetaB under zero strain, whereas different strain-induced resonances appeared under the same applied strain. The origin of different strain-induced resonances was comprehensively investigated by assuming the effective asymmetry and introducing the detuning into the harmonic oscillator model. It was found that the detuning had different influences on FlexMetaF and FlexMetaB, because the different SRRs arrangements resulted in different coupling strength. The findings might improve the understanding on the effects of strain on THz electromagnetic responses in flexible THz metamaterials in terms of their applications in flexible or curved devices.

References

[1] Shelby R A, Smith D R and Schultz S 2001 *Science* **292** 77
[2] Pendry J B 2000 *Phys. Rev. Lett.* **85** 3966
[3] Schurig D, Mock J J, Justice B J, Cummer S A, Pendry J B, Starr A F and Smith D R 2006 *Science* **314** 977
[4] Moser H O, Casse B D F, Wilhelmi O and Saw B T 2005 *Phys. Rev. Lett.* **94** 063901
[5] Chen H T, Padilla W J, Zide J M O, Gossard A C, Taylor A J and Averitt R D 2006 *Nature* **444** 597
[6] Singh R, Cao W, Al-Naib I, Cong L, Withayachumnankul W and Zhang W 2014 *Appl. Phys. Lett.* **105** 171101
[7] Gu C, Qu S B, Pei Z B, Xu Z, Liu J and Gu W 2011 *Chin. Phys. B* **20** 017801
[8] Chen H T, Padilla W J, Cich M J, Azad A K, Averitt R D and Taylor A J 2009 *Nat. Photonics* **3** 148
[9] Manjappa M, Chiam S Y, Cong L, Bettiol A A, Zhang W and Singh R 2015 *Appl. Phys. Lett.* **106** 181101
[10] Xu X, Peng B, Li D, Zhang J, Wong L M, Zhang Q, Wang S and Xiong Q 2011 *Nano Lett.* **11** 3232
[11] Yen T J, Padilla W J, Fang N, Vier D C, Smith D R, Pendry J B, Basov D N and Zhang X 2004 *Science* **303** 1494
[12] Fan J, Sun G Y and Zhu W R 2011 *Chin. Phys. B* **20** 114101
[13] Zhang F, Liu Z, Qiu K, Zhang W, Wu C and Feng S 2015 *Appl. Phys. Lett.* **106** 061906
[14] Pendry J B, Holden A J, Robbins D J and Stewart W J 1999 *IEEE Trans. Microw. Theory Tech.* **47** 2075
[15] Driscoll T, Andreev G O, Basov D N, Palit S, Cho S Y, Jokerst N M and Smith D R 2007 *Appl. Phys. Lett.* **91** 062511
[16] Chen C Y, Un I W, Tai N H and Yen T J 2009 *Opt. Express* **17** 15372
[17] Singh R, Al-Naib I A I, Koch M and Zhang W 2011 *Opt. Express* **19** 6312
[18] Li J, Shah C M, Withayachumnankul W, Ung B S Y, Mitchell A, Sriram S, Bhaskaran M, Chang S and Abbott D 2013 *Appl. Phys. Lett.* **102** 121101
[19] Li J, Shah C M, Withayachumnankul W, Ung B S Y, Mitchell A, Sriram S, Bhaskaran M, Chang S and Abbott D 2013 *Opt. Lett.* **38** 2104
[20] Zheng L, Sun X, Xu H, Lu Y, Lee Y P, Rhee J Y and Song W 2015 *Plasmonics* **10** 1331
[21] Alves F, Karamitros A, Grbovic D and Karunasiri G 2011 *SPIE Photonic Devices+ Applications. International Society for Optics and Photonics* **8119** 8119K-1
[22] Walia S, Shah C M, Gutruf P, Nili H, Chowdhury D R, Withayachumnankul W, Bhaskaran M and Sriram S 2015 *Appl. Phys. Rev.* **2** 011303
[23] Gu J, Singh R, Liu X, *et al.* 2012 *Nat. Commun.* **3** 1151
[24] Jin X R, Park J, Zheng H, Lee S, Lee Y P, Rhee J Y, Kim K W, Cheong H S and Jang W H 2011 *Opt. Express* **19** 21652
[25] Evlyukhin A B, Bozhevolnyi S I, Pors A, Nielsen M G, Radko I P, Willatzen M and Albrektsen O 2010 *Nano Lett.* **10** 4571
[26] Tamayama Y, Yasui K, Nakanishi T and Kitano M 2014 *Phys. Rev. B* **89** 075120
[27] Garrido Alzar C L, Martinez M A G and Nussenzveig P 2002 *Am. J. Phys.* **70** 37